Journal of Power Sources 228 (2013) 159–169

Contents lists available at SciVerse ScienceDirect

Journal of Power Sources

journal homepage: www.elsevier.com/locate/jpowsour

Quantitative analysis of the performance impact of low-level carbon monoxide exposure in proton exchange membrane fuel cells

Guido Bender [1], Michael Angelo*, Keith Bethune, Richard Rocheleau

University of Hawaii, School of Ocean Earth Science and Technology, Hawaii Natural Energy Institute, 1680 East West Road, POST 109, Honolulu, HI 96822, USA

HIGHLIGHTS

- Describes methodology to accurately quantify performance loss from CO.
- Quantifies performance loss at low concentrations and several operating conditions.
- Employs GC to quantify magnitude of conversion for CO to CO_2 at steady state.
- Gives fitting equations and parameters for cell voltage loss/recovery versus time.

ARTICLE INFO

Article history:
Received 19 September 2012
Received in revised form
2 November 2012
Accepted 19 November 2012
Available online 27 November 2012

Keywords:
PEMFC
Carbon monoxide
Overpotential
Oxygen crossover
Gas analysis
CO conversion

ABSTRACT

The performance effect of the hydrogen fuel contaminant carbon monoxide (CO) for dry gas concentrations ranging from 1 to 10 ppm in proton exchange membrane fuel cells (PEMFCs) is reported. Performance loss is investigated for different operating conditions including several temperatures, anode relative humidities, and current densities. An analytical method is presented to quantify performance loss due to CO exposure ($\Delta\eta$), the time required to attain steady state of the CO reaction mechanism (t_{trans}), and the effectiveness of cell performance recovery in neat hydrogen. For select experiments, the magnitude of conversion of CO to carbon dioxide (CO_2) at steady state (ξ_{CO}) is quantified with gas chromatography. The results show (i) $\Delta\eta$ is greatest at high CO concentrations, high current density, and low anode relative humidity, (ii) oxygen crossover from the cathode decreases $\Delta\eta$, and (iii) ξ_{CO} is higher at a temperature of 60 °C than 80 °C. The latter may be attributed to an increased amount of liquid water in the cell increasing the oxygen crossover. The data also shows that recovery in neat hydrogen was typically complete. A summary of all experimental results of $\Delta\eta$ is given in Appendix B as fitting equations and parameters to assist in cell performance model development.

© 2012 Elsevier B.V. All rights reserved.

1. Introduction

Proton exchange membrane fuel cells (PEMFCs) are promising clean power sources for transportation and stationary applications. When operated with pure hydrogen as the fuel and clean air as the oxidant, PEMFCs offer high efficiencies, high power densities, and zero emissions [1,2]. However, contaminants in the hydrogen fuel stream (e.g. CO, CO_2, H_2S, NH_3, and organic compounds) and/or in the air stream (e.g. NO_x, SO_x, CO_2, NH_3 and organic compounds) have been shown to affect fuel cell performance, sometimes resulting in permanent damage to the membrane electrode assemblies (MEAs) [3–5]. Numerous studies have been reported that characterized the effect of contaminants on cell performance, proposed reaction mechanisms for contaminants entering the fuel cell, and described models that predicted their effects on cell performance. The majority of these works focused on CO at concentration levels between 10 and 100 ppm. At these concentrations significant performance loss was observed. However, based on experiments conducted to support the development of the draft hydrogen fuel quality specification, SAE J2719, it is currently believed that contaminant concentration limits for CO as low as 0.2 ppm may be required to maintain acceptable cell performance levels [6].

A significant detail in assessing the impact of CO at concentrations below 10 ppm is the accurate determination of the performance loss in neat H_2/air due to cell degradation. This loss is expected to vary significantly with operating conditions but may

* Corresponding author. Hawaii Sustainable Energy Research Facility (HI-SERF), Hawaii Natural Energy Institute (HNEI), University of Hawaii at Manoa, 929 Cooke Street, Honolulu, HI, USA 96813. Tel.: +1 (808) 593 1714; fax: +1 (808) 593 1719.
E-mail address: mangelo@hawaii.edu (M. Angelo).
[1] Current address: National Renewable Energy Center, Golden CO, USA.

0378-7753/$ – see front matter © 2012 Elsevier B.V. All rights reserved.
http://dx.doi.org/10.1016/j.jpowsour.2012.11.062

also, as shown in this work, vary between MEAs from the same vendor and production batch. To address this issue, we developed a quantitative methodology that separates the cell degradation from the performance loss induced by a contaminant. The method is applicable to any operating condition with MEAs of any loading, batch, or manufacturer. It enables comparison of the contaminant induced performance impacts over a wide range of operating conditions.

In this work, we report on this method and apply it to quantify the performance impact of CO at dry gas concentrations of 1, 2, and 10 ppm and several operating conditions to affirm the proposed SAE J2719 gas purity requirements. The overpotential change of the cell due to CO exposure ($\Delta\eta$), the time required to attain steady state of the CO reaction mechanism (t_{trans}), and the effectiveness of performance recovery in neat hydrogen are reported and discussed for each operating condition which included various temperatures, relative humidity, and current densities. The role of crossover oxygen in affecting $\Delta\eta$ and t_{trans} is also investigated and the magnitude of CO to CO_2 conversion when the CO reaction mechanism attained steady state is reported for certain experiments.

2. Experimental

Experiments discussed in this work were performed at the Hawaii Fuel Cell Test Facility (HFCTF), a state of the art laboratory for fuel cell research on single cells and short stacks. HFCTF features on-site production of high-purity hydrogen, on-site air purification and supply, and a suite of diagnostic equipment. FCATS™ G050 series test stations from Green Light Power Technologies Inc. modified for on-line gas analysis at the anode and cathode were used to conduct experiments on 50 cm^2 single cell PEMFCs. Continuous 1 kHz resistance measurements were recorded during all polarization and constant current experiments using a Model DOT-1000 Milli-Ohmmeter from Criterion Instruments. A detailed description and schematic of this experimental setup was reported [7]. Careful management of humidification, temperature, and gas flow control systems assured stable long-term operation of PEMFCs [7].

Table 1 summarizes the fuel cell hardware and component materials used in this work. Commercially available membrane electrode assemblies (MEA) with 0.375 mg Pt cm^{-2} loading and 50% Pt/C catalysts were purchased from Ion Power. Membrane and electrode thicknesses were, 40 μm and 20 μm, respectively, and were determined from MEA cross sections via scanning electron microscopy (SEM). The cells were assembled using 25 BC gas diffusion layers (GDL) from SGL Technologies on both electrodes. Standard protocols were employed for cell assembly, conditioning, and diagnostics. Prior and subsequent to contaminant testing, beginning of test (BOT) and end of test (EOT) diagnostics were performed on the cell. Diagnostics included polarization curves with H_2/air and H_2/O_2 (VI curves).

Table 2 summarizes the operating conditions used in this work. H_2/air and H_2/O_2 polarization curves were obtained using ultra-high purity gases humidified prior to flowing into the anode and cathode of the cell. Polarization curves were measured in current control mode, starting at a current density of 1.2 A cm^{-2} with 0.2 A cm^{-2} steps towards open circuit (OC). Cells were operated at a flow stoichiometry of two at the anode and cathode for each current density when air was the oxidant gas. For curves measured with O_2, the flow rates were the same as those in the air curves resulting in a cathode stoichiometry of 9.5. An additional data point was recorded at 0.1 A cm^{-2}. Anode and cathode flow rates at this measurement point were equivalent to the flows at a current density of 0.2 A cm^{-2}. At each point, the current was held constant for 15 min. The voltage values reported were averaged over the last 5 min. The cell was subsequently held for 1 min at OC and the maximum recorded voltage was used as the open circuit voltage.

Long duration constant current density experiments were conducted at fixed operating conditions to enable the quantification of the magnitude of performance loss due to CO exposure. The voltage change of cells operating continuously in current control mode for durations of 100–200 h with neat H_2/air was measured at different conditions to characterize the performance loss of the MEA.

For CO exposure experiments, the cell was operated for a period of time with neat hydrogen and air followed by a period where a dry gas mixture of hydrogen and CO was continuously injected into the humidified neat hydrogen stream. The specified humidification was maintained by increasing the temperature of the humidifier to compensate for the dry contaminant injection.

Table 1
Cell hardware and components.

Hardware	General	
	Anode	Cathode
MEA	Ion power	
Area	50 cm^2	
Membrane thickness	40 μm	
Electrode thickness	20 μm	20 μm
Flow-field	2 Channel serpentine	3 Channel serpentine
Catalyst	50% Pt/C	50% Pt/C
Loading	0.375 mg Pt cm^{-2}	0.375 mg Pt cm^{-2}
GDL	SGL-BC25	SGL-BC25
Gaskets	178 μm, Teflon	203 μm, Teflon

3. Methodology

This section describes how ξ_{CO}, $\Delta\eta$, and t_{trans} were calculated. Values for ξ_{CO} were quantified from CO and CO_2 concentrations measured using gas chromatography at the anode inlet and outlet. The molar flow rates of CO and CO_2 entering and exiting the fuel cell were quantified following the equations given in [7] and used to determine the quality of closure for the carbon balance (Q_{CBal}). Q_{CBal} was calculated using Eq. (1), where $\bar{\dot{n}}_{i,out}$ and $\bar{\dot{n}}_{i,in}$ represent the total molar flow rate of carbon containing impurity species out of and into the electrode, respectively. A value of one indicates complete closure of the molar flow balance of carbon at the anode.

$$Q_{CBal} = \frac{\sum_i \bar{\dot{n}}_{i,out}}{\sum_i \bar{\dot{n}}_{i,in}} \quad (1)$$

The conversion of CO to CO_2 at steady state was calculated using Eq. (2). The calculation assumes closure of the mass balance, which was validated in previous work where the C mole balance closed to within 3% [7]. ξ_{CO} was calculated as shown in Eq. (2), where ξ_{CO} was the conversion of CO, $\bar{\dot{n}}_{COin}$ and $\bar{\dot{n}}_{COout}$ were the molar flow rates of CO entering and exiting the cell, respectively.

$$\xi_{CO} = \frac{\bar{\dot{n}}_{COin} - \bar{\dot{n}}_{COout}}{\bar{\dot{n}}_{COin}} \quad (2)$$

Table 2
Operating conditions.

Operating conditions	General	
	Anode	Cathode
Relative humidity	100/80/60%	50%
Stoichiometry	2	2
Fuel/oxidant	H_2	Air/oxygen/hydrogen
Pressure	48.3 kPa_g	48.3 kPa_g
Temperature	80/60 °C	
Current Density	1/0.6/0.2 A cm^{-2}	

This section describes the experimental and analytical methodology developed to quantify the impact of trace level contaminants on fuel cell performance. The methodology separates the performance loss that occurs during operation with neat H_2/air from that caused by the contaminant. It also provides specific procedures for determining $\Delta\eta$ and t_{trans}.

Fig. 1 shows the measured cell voltage data (black, left axis) and $\Delta\eta$ (grey, right axis) for an experiment conducted at constant current with 1 ppm CO. Conditions are given within the figure. The experiment is divided into three distinct phases which are labeled in Fig. 1.

- Phase 1 is the pre-poisoning period conducted with neat H_2/air. The performance decay during this phase is used to extrapolate the projected performance decay of the cell under neat H_2/air operation for a time equivalent to the duration of the entire experiment (i.e. Phases 1 through 3). The length of Phase 1 required to achieve accurate extrapolation is approximately 1/3 of the length of the entire experiment. The quantification of the fitting interval is discussed in Appendix A. Performance loss during Phase 1 is attributed to changes in the MEA.
- Phase 2 begins with the introduction of contaminant into the anode feed stream. In the experiments reported in this work, contaminant concentration was held constant throughout Phase 2. Performance loss during this phase includes the losses due to MEA effects which were estimated by extrapolation of the Phase 1 data plus the loss due to the contaminant. Performance loss occurring during operation with pure gases was assumed to be continuous and independent of losses resulting during exposure to contaminants.
- Phase 3, the recovery period, begins when the flow of the contaminant is stopped and operation on neat H_2/air is resumed. Performance changes during this phase include continuing losses due to degradation of the MEA plus the performance recovery resulting from the reaction of CO to CO_2 and CO desorption.

Analysis of the data from all three phases allows the performance impact due to contaminant exposure to be accurately quantified by separating it from the performance decrease due to MEA degradation. It also enables accurate determination of the extent of recovery following removal of the contaminant from the fuel stream. All contaminant experiments were analyzed in this manner.

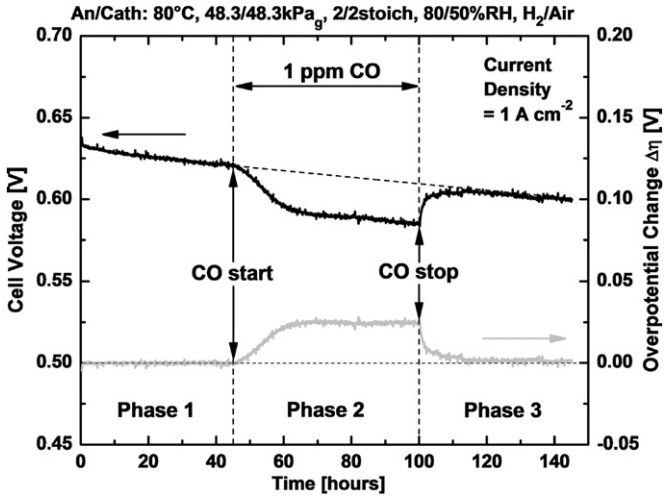

Fig. 1. Top: experimentally measured cell data versus time for exposure to dry gas concentration of 1 ppm CO at 45 h. Extrapolated fit of pre-poisoning period throughout experimental duration shown as dashed line (- - -). Bottom: calculated values for overpotential change ($\Delta\eta$) versus time due to CO exposure.

Fig. 1 illustrates the application of the methodology described above. The top line shows the measured cell voltage response while the bottom line shows the calculated change in cell overpotential attributed to the CO, i.e. $\Delta\eta$. Phase 1, lasted from 0 to 45 h which represented approximately 1/3 of the duration of the experiment and showed the measured cell voltage under neat H_2/air operation. The Phase 1 data was fitted using Eq. (3) to extrapolate the performance degradation through the test time of 145 h. Eq. (3) is purely empirical and consists of an exponential and linear component since it was determined to achieve the best overall fit to the data from several different types of fitting equations. The extrapolated data is represented by the dashed line (- - -) in the top graph in Fig. 1.

$$V_{Fit}(t) = p_1 \cdot \exp\left(-\frac{t}{p_2}\right) + p_3 + t \cdot p_4 \quad (3)$$

with $p_1 \geq 0$, $p_2 > 0$, $p_3 > 0$, $p_4 < 0$

Although the projected fit and the cell performance after recovery are in good agreement, it is important to note that this 'front-loaded' fitting procedure relied entirely on data prior to contaminant exposure. Results at our facility and other research institutions have shown that performance recovery in neat H_2/air subsequent to exposure to a contaminant may remain incomplete [8–10]. Thus, performance at the end of the recovery phase (Phase 3) cannot be used for data fitting. For each experiment, the reliability of the 'front-loaded' fit was qualitatively assessed using three criteria: (i) there was no significant deviation of $\Delta\eta$ from zero over the pre-poisoning period, (ii) the calculated overpotentials did not contain any negative values, which would indicate an overcompensation of the performance degradation of the fuel cell by the fit, and (iii) during the final stages of cell recovery a constant overpotential was observed.

During phase 2, from 45 to 100 h, 1 ppm of CO was continuously supplied to the fuel inlet stream. Upon introduction of the CO, the rate of loss in cell performance increased significantly due to CO adsorption reducing the active Pt reaction sites available for the hydrogen oxidation reaction (HOR). As the reactions with CO that were involved in catalyst poisoning attained steady state, the measured rate of performance loss became identical to the rate of performance loss from the extrapolated fit of Phase 1. The measured cell voltage data in Fig. 1 indicated that steady state conditions were reached at approximately 70 h and were maintained until the contaminant flow was stopped, at 100 h of operation.

Phase 3, the recovery phase was initiated at 100 h by stopping the flow of the contaminant and returning to operation with neat H_2/air which was continued until the experiment was terminated at 145 h. During this phase, the cell performance initially recovered rapidly and then asymptotically approached the MEA performance predicted by the extrapolated fit of Phase 1. This indicated that the performance recovery at these operating conditions was nearly complete.

Overpotential change ($\Delta\eta$) data was calculated by subtracting the measured cell voltage from the extrapolated neat H_2/air performance (Eq. 4). The $\Delta\eta$ data is represented by the lower line in Fig. 1.

$$\Delta\eta(t_i) = V_{Fit}(t_i) - V_{cell}(t_i) \quad (4)$$

During Phase 1, under neat H_2/air operation, the calculated $\Delta\eta$ was zero, as expected. Following introduction of the CO into the hydrogen stream in Phase 2, the $\Delta\eta$ increased rapidly, and approached a steady state value of 25 mV. It is important to note

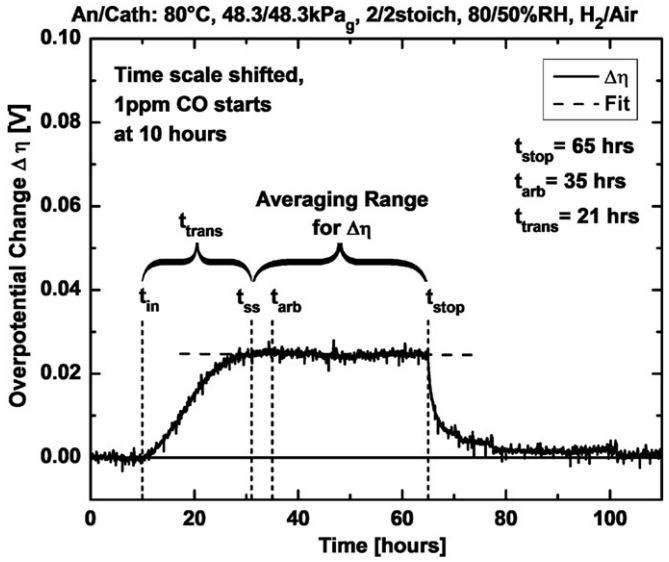

Fig. 2. Example of quantitative analysis of processed contaminant data to determine t_{trans}, the time period until steady state conditions are reached and $\Delta\eta$, the overpotential change due to contamination.

that the performance degradation due to CO exposure is similar in magnitude to the projected neat hydrogen loss over the same period of time. This emphasized the need for a methodology that separates the performance impact of CO from the performance degradation due to neat H_2/air operation.

We also developed a procedure to estimate the time required for the poisoning process to reach steady state, which we refer to as the transient time of the poisoning process t_{trans}. To facilitate comparison of the overpotential data from experiments with different times before poisoning (Phase 1) overpotential data are shown so that the contaminant injection appears to begin at 10 h. Fig. 2 shows $\Delta\eta$ for the experiment shown in Fig. 1 plotted in this manner. A five-step process was developed to reproducibly estimate t_{trans} and $\Delta\eta$. The methodology is illustrated in Fig. 2 using the data of the contaminant experiment shown in Fig. 1:

(1) Identify an arbitrary time, t_{arb}, that is near the beginning but clearly within the steady state region. In this region, $\Delta\eta$ typically exhibits a linear progression with a slope near zero.
(2) Apply a linear fit from t_{arb} to the end of the contaminant injection, t_{stop}.
(3) Plot the fit and the change of overpotential data into the same graph and identify the time, t_{ss}, when the value of $\Delta\eta$ and the linear fit begin to diverge. This time indicates when steady state has been reached.
(4) Subtract the time of the contaminant injection, t_{in}, from t_{ss} to determine the transient time, t_{trans}, required to reach steady state.
(5) Average the $\Delta\eta$ data between t_{trans} and t_{stop} to determine $\Delta\eta$ at steady state.

In the data shown in Fig. 2, the rate of change in $\Delta\eta$ significantly slowed and approached a slope of 0 at approximately 30 h. This indicated the approximate onset of steady state. The arbitrary time t_{arb} was selected to be 35 h to assure the fit would be well within the steady state region. The data from t_{arb} (35 h) to the end of the contaminant injection ($t_{stop} = 65$ h) was fitted using a linear regression. The fit was represented by the dashed horizontal line shown in Fig. 2. Deviation of the fit from the $\Delta\eta$ data indicated that steady state conditions were reached at 31 h and thus t_{trans} was 21 h. The change in overpotential due to CO exposure at steady state was determined by averaging $\Delta\eta$ from 31 to 65 h and found to be 25 mV. Values for $\Delta\eta$ for CO concentrations between 1 and 10 ppm at several conditions are presented in the following section. These results are expected to be of significant value for the determination of reaction rate constants and contaminant model verification.

4. Results and discussion

In this section, we present data and discuss the effects of CO concentrations of 1, 2, and 10 ppm at different operating conditions on $\Delta\eta$, t_{trans}, ξ_{CO}, and the performance recovery in neat H_2/air. Unless otherwise noted CO concentrations are reported as dry gas concentrations. Experiments discussed in this section were performed with PEMFCs operated at the conditions given in Table 3, which also provides a summary of all quantitative results including $\Delta\eta$, t_{trans}, Q_{CBal}, and ξ_{CO}. Data were analyzed using the methodology described in Section 3.

4.1. Effect of CO on cell overpotential and transient time

Fig. 3 shows $\Delta\eta$ versus time for cells exposed to 2 ppm CO at current densities of 0.2, 0.6, and 1.0 A cm^{-2}, at a cell temperature of

Table 3
Transient time t_{trans} and overpotential change $\Delta\eta$ for 1, 2, and 10 ppm CO at various operating conditions.

[CO] [ppm]	ECA [m^2 g$_{Pt}^{-1}$]	Temp. (°C)/Anode R.H. (%)	Current density [A cm^{-2}]	Cathode gas	t_{trans}[h]	$\Delta\eta$ [mV]	Q_{CBal}[%]	ξ_{CO}[%]
2	84.07	60/100%	1	Air	14	246	98.1	70.3
2	71.87	60/100	0.6	Air	29	159	–	–
2	85.12	60/100	0.2	Air	69	19	–	–
2	72.32	60/100	1	O_2	n/a	35	–	–
2	73.28	60/100	1	H_2	n/a	300	–	–
1	65.12	80/100	1	Air	25	25	–	–
2	69.28	80/100	1	Air	14	45	–	–
10	69.33	80/100	1	Air	9	241	110.9	33.4
1	88.89	80/80	1	Air	22	25	–	–
2	80.25	80/80	1	Air	13	48	–	–
10	83.88	80/80	1	Air	13	238	106.5	21.1
1	85.94	80/60	1	Air	36	27	–	–
2	71.98	80/60	1	Air	13	77	96.9	43.7
10	83.47	80/60	1	Air	12	323	102.3	32.8
1	60.94	60/100	1	Air	29	173	100.6	61.7
10	85.84	60/100	1	Air	8	343	97.7	91.3

60 °C, and an anode relative humidity of 100%. It should be noted that the recovery phase in pure H_2 was not performed for the 0.2 A cm^{-2} experiment. The results showed a significant decrease of t_{trans} with increasing current density. Compared to a current density of 1.0 A cm^{-2}, t_{trans} was 2.1 and 4.9 times greater for the 0.6 and 0.2 A cm^{-2} experiments, respectively. Because the flow stoichiometry and injection concentration of CO were held constant, the absolute flow rate and thus the contaminant molar flow rate into the cell was reduced by a factor of 1.7 and 5.0, for the 0.6 and 0.2 A cm^{-2} experiments, respectively. This suggested a directly proportional relationship between the molar flow rate of CO into the cell and t_{trans}.

A significantly greater performance loss was observed at higher current densities. The value for $\Delta\eta$ at the current densities of 0.2, 0.6, and 1 A cm^{-2} was 19, 159, and 246 mV, respectively. This increase of $\Delta\eta$ with current density likely resulted from the competitive adsorption of CO and hydrogen. At higher current densities a greater fraction of the electrochemically active surface area was required to sustain the hydrogen oxidation reaction, which in the presence of CO, decreases cell voltage. For these experiments, the exact Pt–CO or Pt–H surface coverage was not known; however, the trend of increased overpotential for a fixed CO concentration at higher operating current densities was consistent with the modeling predictions of previous reports for higher CO concentrations ($\geq$10 ppm) [3,4,11].

4.2. The role of crossover oxygen on the oxidation of CO

Some of the CO that adsorbs to the Pt/C catalyst within the fuel cell reacts to form CO_2. Various studies have reported that the reaction of CO to form CO_2 may proceed via a chemical reaction, an electrochemical reaction, or a combination of the two. A generally accepted mechanism for the electrochemical oxidation of CO that was linearly adsorbed onto Pt is given by Eqs. (5) and (6) [4], [11–13].

$$CO + Pt \leftrightarrow Pt - CO_{ads} \quad (5)$$

$$Pt - CO_{ads} + H_2O \rightarrow Pt + CO_2 + 2H^+ + 2e^- \quad (6)$$

A similar mechanism has been reported for the electrochemical oxidation of CO that was bridge bonded on Pt [12]. In either of these cases water was considered to be the source of oxygen for the electrochemical oxidation of CO.

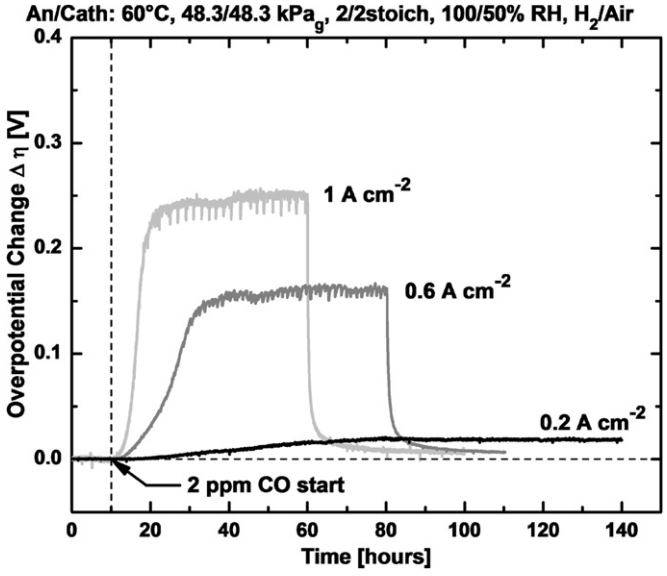

Fig. 3. Comparison of overpotential change ($\Delta\eta$) versus time for cells exposed to dry gas concentration of 2 ppm CO at 60 °C; 0.2, 0.6, and 1 A cm^{-2}.

Literature has indicated that the electro-oxidation of CO requires a potential of at least 350 mV on a platinum/ruthenium alloy catalyst versus a reversible hydrogen electrode (RHE) [14–16] to occur. For fuel cells using Pt/C as the catalyst, such as those in this work, the ignition potential for CO electro-oxidation is expected to be even higher. As shown in Table 3, the maximum value for $\Delta\eta$ measured in this work was 343 mV for a 10 ppm CO exposure at 60 °C and an anode relative humidity of 100%. Most of the $\Delta\eta$ values calculated were substantially lower. Previous work has also shown that the potential for the onset of the CO electro-oxidation and its peak potential are dependent on cell temperature and cell humidification. Both were reported to decrease with increasing cell temperature [14,15]. Furthermore, the CO stripping peak potential was shown to increase when the working electrode of the cell was operated with a less than fully humidified gas feed stream [16]. Therefore, the overpotentials calculated in this work are likely below the potential onset of CO electro-oxidation, and are thus unlikely to occur.

A second possible mechanism for CO oxidation is a chemical reaction with oxygen which enters the anode by diffusing across the MEA from the cathode. The impact of crossover oxygen on the oxidation of platinum adsorbed CO has gained importance in recent years since the thickness of proton exchange membranes in fuel cells has significantly decreased from 180 to 25 μm which has thereby increased the rate of oxygen crossover. Evidence of oxygen crossover and reaction with CO was given by Zhang et al. [17], who reported that reaction of CO to CO_2 may occur as a catalytic surface redox mechanism such as that shown by Eqs. (7) and (8), or through the formation of adsorbed hydroxyls, OH_{ads}, that react further with surface bound CO electrochemically as shown in Eqs. (9) and (10).

$$O_2 + 2Pt \leftrightarrow 2(Pt - O_{ads}) \quad (7)$$

$$Pt - O_{ads} + Pt - CO_{ads} \rightarrow 2Pt + CO_2 \quad (8)$$

$$Pt - O_{ads} + Pt - H_{ads} \leftrightarrow Pt - OH_{ads} \quad (9)$$

$$Pt - OH_{ads} + Pt - CO_{ads} \rightarrow 2Pt + CO_2 + H^+ + e^- \quad (10)$$

To further investigate the role of oxygen as a possible reactant with CO at low concentrations, experiments were performed with different cathode gas compositions which included 100% hydrogen or 100% oxygen. Fig. 4 shows the change in cell overpotential versus time for a cell operated at 60 °C, 1 A cm^{-2}, an anode relative humidity of 100% and 2 ppm CO in the fuel stream. The cathode inlet humidity was 100% when hydrogen was supplied to the cathode and the cell was operated in an electrically driven mode. The cathode inlet humidity was 50% when air or O_2 was supplied to the cathode and the cells were operated galvanically. The values for $\Delta\eta$ were 300, 250, and 35 mV, when the cathode gas was hydrogen, air, or oxygen, respectively. Clearly, the presence and concentration of oxygen at the cathode significantly reduced $\Delta\eta$. Oxygen crossing over from the cathode to the anode presumably reacted with the CO to form CO_2. Based on the $\Delta\eta$ values we believe that the reaction was a chemical process such as that given by Eqs. (7) and (8). More work is required to characterize and quantify the impact of crossover oxygen to gain a greater understanding of the how oxygen on the cathode affects the performance of a PEMFC with CO in the anode feed, specifically at low CO contaminant concentrations.

Fig. 5 shows $\Delta\eta$ data calculated at steady state with the method discussed above for 1, 2, and 10 ppm dry CO concentration exposures at several operating conditions. To allow for more accurate

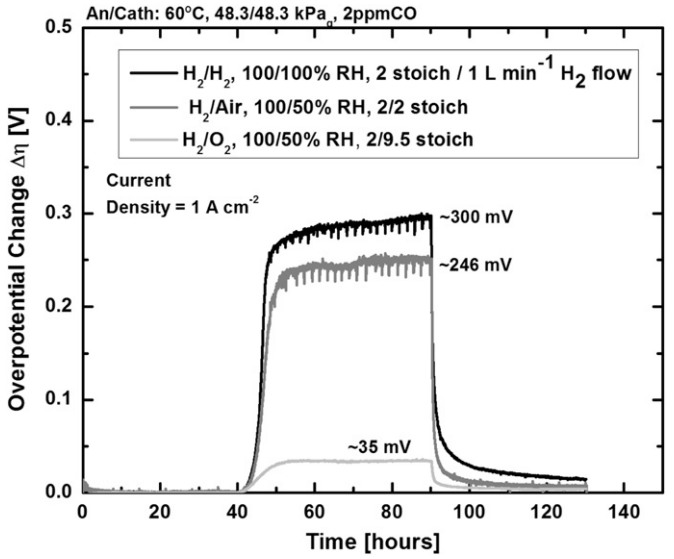

Fig. 4. Comparison of overpotential change ($\Delta\eta$) for cells exposed to dry gas concentration of 2 ppm CO at 60 °C, and (i) H_2/H_2, (ii) H_2/air, and (iii) H_2/O_2 anode/cathode reactant gases.

comparisons the contaminant concentrations were calculated to account for the amount of water vapor in the inlet gas stream. Operating conditions included a 60 °C cell temperature with an anode inlet humidity of 100%, and a cell temperature of 80 °C with anode inlet humidities of 100, 80, and 60%. The results showed that $\Delta\eta$ increased with CO concentration at all operating conditions. This confirmed that, as previously discussed, higher concentrations of CO generally resulted in greater performance losses. The values for $\Delta\eta$ were lower at 80 °C than at 60 °C. This may have indicated that the CO coverage on the Pt catalyst is higher at lower operating temperatures due to thermal kinetic effects. However, the partial pressure of water was 27.4 kPa lower at 60 °C which increased the actual concentration of CO in the feed stream and may have increased the equilibrium surface coverage. Water transport within the cell may have affected the transport of oxygen, which as shown in Fig. 4, mitigates performance loss.

Fig. 6 was included to emphasize how the mass transport limitations changed with operating conditions for the particular cell design, GDL, and MEA used in this study. The figure shows fuel cell performance curves and 1 kHz resistances measured at 80 and 60 °C with 100% humidity at the anode inlet and 50% humidity at the cathode inlet. No change in the cell resistance was observed at 80 or 60 °C; however, a significant performance deviation was apparent at current densities above 40 mA cm^{-2}. This indicated that the performance at 60 °C was impacted by higher cathode mass transport limitations. Considering Figs. 5 and 6 together, the results suggested that the physical state of water within the cell may have also affected the cell performance when CO was present.

Fig. 5 also shows $\Delta\eta$ values of cells that were operated with different anode humidities. The data did not show a clear trend with humidification. At CO concentrations near 1 ppm $\Delta\eta$ was similar for all anode humidification conditions. At higher CO concentrations a humidity of 60% resulted in the largest performance loss and the lowest performance loss was observed at 80%. The exact reasons for the different values of $\Delta\eta$ are not known since many of the processes that take place within the fuel cell are interlinked which makes it difficult to clearly identify trends of $\Delta\eta$ with certain operating parameters. In general though, the trends observed here with $\Delta\eta$ and operating conditions are consistent with those reported previously for contaminant concentrations $\geq$10 ppm CO [3,4,7,18].

Fig. 7 shows results for the conversion of CO to CO_2, ξ_{CO}, determined by gas chromatography at steady state conditions for selected experiments. The CO concentration values in the figure account for the water pressure in the humidified gas stream. For 60 °C, ξ_{CO} increased with CO concentration. This trend was similar to that observed in Fig. 5 for $\Delta\eta$. It indicated that higher concentrations were likely related to an increased rate of reaction due to higher Pt–CO catalyst coverage. The conversion of CO was consistently lower at 80 °C. This may be directly related to a lower catalyst coverage of CO at the higher temperature and/or indirectly related to higher amounts of liquid water at 60 °C. According to Basura et al. the presence of liquid water enhances the transport of oxygen across the MEA [19], and according to Zhang et al., the presence of oxygen at the anode increases the chemical oxidation of CO to CO_2 [17]. Both together would consequently result in an increased ξ_{CO}.

Other literature shows that the oxygen crossover rate is also dependent on the operating conditions of the fuel cell. The oxygen

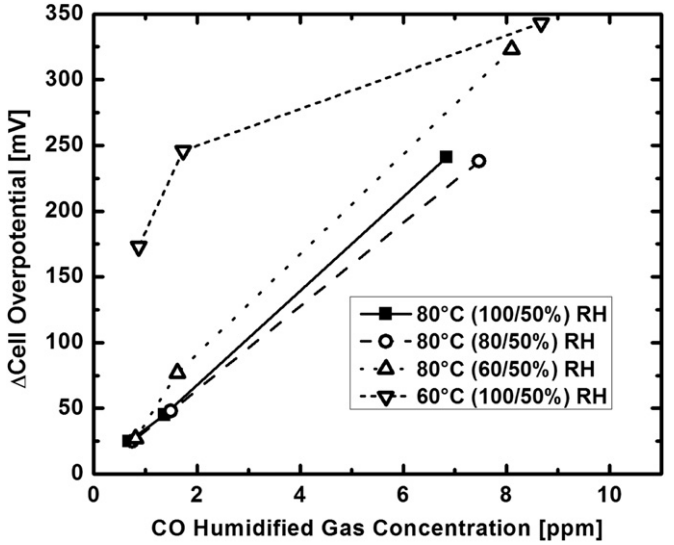

Fig. 5. Comparison of overpotential change ($\Delta\eta$) at steady state for cells exposed to dry gas concentrations of 1, 2, 10 ppm CO at several operating conditions.

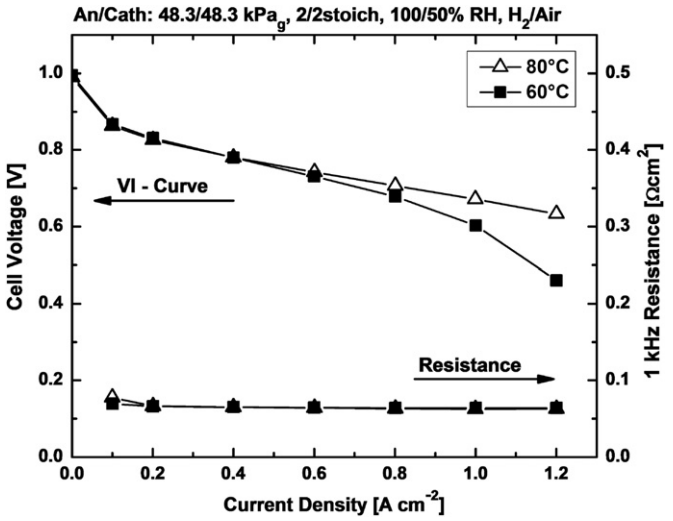

Fig. 6. VI curves and 1 kHz resistances for fuel cells operated at 80 and 60 °C with an anode/cathode humidity inlet humidity of 100/50%.

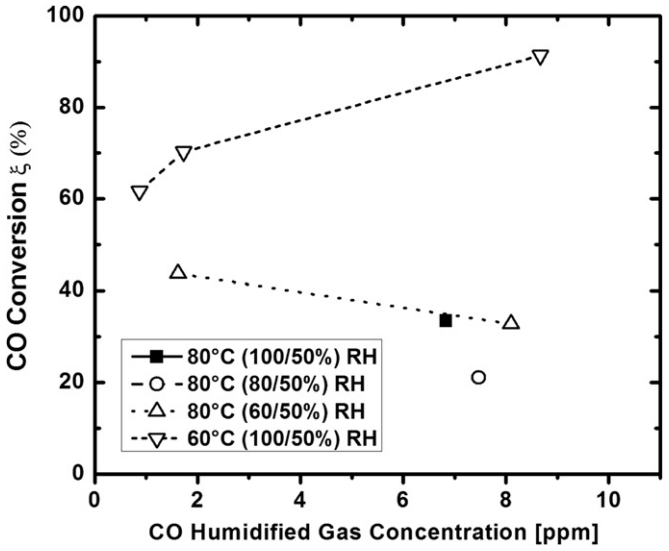

Fig. 7. Magnitude of CO to CO_2 conversion quantified from gas chromatography data at different operating conditions.

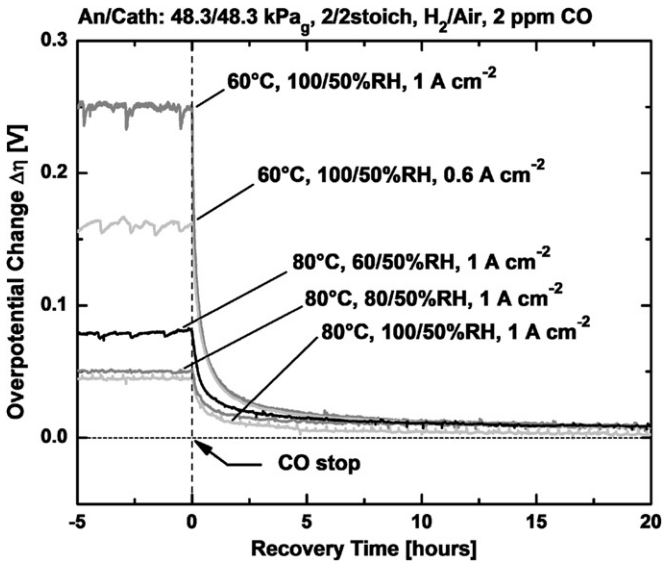

Fig. 9. Comparison of overpotential change ($\Delta\eta$) versus recovery time for dry CO gas concentration of 2 ppm and several operating conditions which are given within the figure.

crossover rate was reported to increase with temperature, with the relative humidity of the fuel cell, and with the cathode oxygen concentration [19–22]. Ma et al., suggested that the permeability of oxygen in Nafion is mainly influenced by thermal diffusion [20], while, as mentioned above, Basura et.al concluded that the oxygen diffusion coefficient is related to the water content of the membranes and suggested that the aqueous phase is dominantly involved in the diffusion pathway [19]. A comparison of the results in Figs. 6 and 7 may confirm the literature results since they respectively show an impact of liquid water on the cell performance and an increase of the conversion of CO to CO_2.

4.3. Self-induced recovery

Fig. 8 shows data for the transition from phase 2, the CO exposure phase, to phase 3, the recovery phase in neat H_2 and air. The time scale in the figure is shifted so that the recovery phase starts at 0 h. The data indicated a decrease in $\Delta\eta$ versus time when switching from 1, 2, and 10 ppm CO exposure to neat H_2/air operation. Although $\Delta\eta$ at steady state varied from 173 to 343 mV as CO concentration increased from 1 to 10 ppm, the recovery of the three cell voltages is nearly identical. During the first hour of recovery $\Delta\eta$ decreased significantly and then asymptotically approached values that were only a few mV above zero over several tens of hours. This indicated nearly complete performance recovery for these concentrations and operating conditions without an externally driven recovery process. The shape and similarity of the $\Delta\eta$ plots was indicative of rapid CO desorption from the catalyst surface upon reintroduction of the neat hydrogen. The time scale for performance recovery in pure H_2 appeared to be independent of the CO concentration at these operating conditions and concentrations.

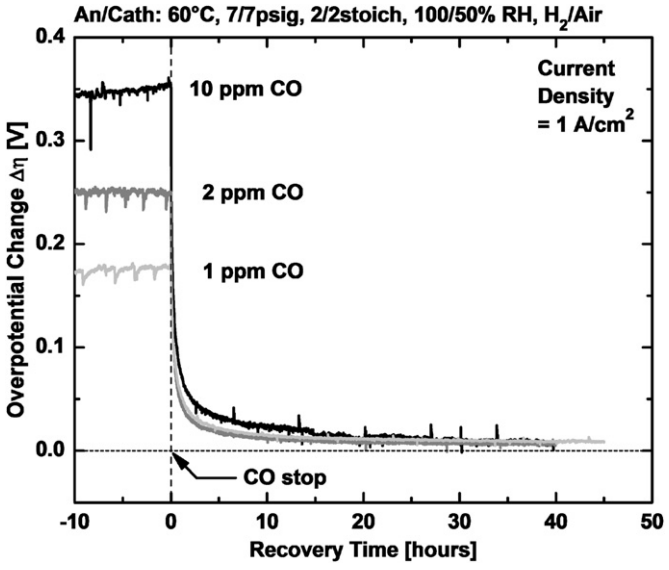

Fig. 8. Comparison of overpotential change ($\Delta\eta$) versus recovery time for dry CO gas concentrations of 1, 2, and 10 ppm, 60 °C and 100% relative humidity.

Fig. 9 shows this self-induced recovery for a variety of operating conditions following poisoning with 2 ppm CO. Conditions include cell current densities of 0.6 and 1.0 A cm^{-2} at 60 °C, and anode/cathode relative humidity of 60/50, 80/50, and 100/50% at 80 °C. Again the time scale was shifted so that the recovery phase started at 0 h. The data indicated two trends with operating conditions: lower cell temperature and lower anode humidification resulted in a slower recovery process. The temperature effect was expected, since the desorption rate is strongly temperature dependent and increases with increasing temperature. At lower humidification, however, while considering similar conversion of CO, as shown in Fig. 9, a reduced activity of water may have contributed to this effect. In any case, the data indicated that the operating conditions tested in this work did not have a significant effect on the completeness of performance recovery. All cells attained significant performance recovery within the first five hours of being subjected to neat hydrogen.

5. Conclusions

An analytical methodology was developed that enabled accurate quantitative determination of the performance loss associated with the presence of low-level CO contaminants (≤10 ppm) within the anode feed stream of a PEMFC. The methodology enabled

comparison of the contaminant impact between different MEAs, MEAs operated at various conditions, and MEAs exposed to different contaminant concentrations. The methodology divided the experiment into three distinct phases: a pre-poisoning phase, a poisoning phase, and a recovery phase with the minimum duration of the pre-poisoning being approximately 1/3 of the entire experiment duration. Extrapolation of the pre-poisoning data then allowed accurate prediction of the neat H_2/air performance degradation of the cell. It also enabled us to separate and accurately determine the degradation due to contaminant exposure in the same experiment.

The impact of dry gas concentrations of 1, 2, and 10 ppm CO on the cell performance over a wide range of operating conditions was studied by combining the developed methodology with a previously described high-resolution gas analysis technique. Over the concentration range studied, the greatest performance impact was found to occur at high contaminant concentration, low cell temperature, low anode relative humidity, and high current density. While cell temperature had the most effect, the self-induced performance recovery from the steady state poisoning state operating conditions was found to be much less dependent on operating conditions or contaminant concentration. Lower temperatures resulted in longer recovery times although the final performance recovery was similar regardless of operating conditions and led to nearly complete recovery after approximately 5 h of recovery time.

Comparison of CO exposure experiments with different cathode reactants of hydrogen, air, and oxygen provided strong evidence that oxygen permeating through the membrane from the cathode to the anode significantly reduced the impact of the CO on cell performance. The crossover oxygen was believed to enhance the conversion process of CO to CO_2. The conversion of CO to CO_2 at steady state decreased with increased operating temperature of the fuel cell. This may have been related to increased oxygen crossover due to increased amounts of liquid water in the cell at lower temperatures.

This work provided evidence that the complexity of the CO contamination process increased for low CO concentration levels with respect to previous studies at higher concentrations. Oxygen crossover, the presence of liquid water, the thickness of the membrane, the catalyst loading and transient operating conditions will have to be accounted for in future hydrogen fuel quality specifications. Additional model development and experiments at the fuel purity recommendations from the Society of Automotive Engineers (SAE) and the International Organization for Standardization (ISO) working committees are needed. Future work at our laboratory will address the experimental aspects of these needs while Appendix B provides numerical fits to the data presented in this paper which we hope will provide modelers access to valuable data for further elucidation of CO contamination processes.

Acknowledgements

The authors are grateful for financial support received from the United States Department of Energy/National Renewable Energy Laboratory through grant No. ZFH-7-77611-01. We would also like to thank Chuck Fraley for performing the gas chromatograph measurements and Dr. Jean St-Pierre for a critical review on the manuscript. The ongoing support of the Hawaiian Electric Company (HECO) to the operations at the Hawaii Fuel Cell Test Facility is greatly appreciated.

Appendix A. Methodology for analysis of cell voltage response

To determine the range of cell performance degradation for PEMFCs operated with neat H_2/air over the maximum length of a contamination experiment several MEAs from the same production batch were tested at various operating conditions. The test duration was 200 h, which was the maximum experimental time of this work. The results of three experiments are shown in Fig. 10. Each of the plots represents the performance of a different MEA over time with the exception of the plot where the performance measurement was interrupted. In this case, the cell was shut down at 100 h, then restarted and operated for an additional 100 h to measure the performance degradation before and after shutdown. The operating conditions are given within the figures.

Also shown in Fig. 10 are the performance degradation rates calculated from a linear regression of the data. For the cell shutdown after 100 h the linear degradation rate was 240 $\mu V\,h^{-1}$ before and after shutdown indicating that the cell could be stopped and restarted without affecting the degradation rate. The linear degradation rate for the other MEA operated at 80 °C and 100 % relative humidity was 51 $\mu V\,h^{-1}$. This indicated that a range of degradation rates could be observed for MEAs from the same production batch operated at identical conditions. The MEA operated at 60°C had a degradation rate of 125 $\mu V\,h^{-1}$. This suggested that the MEA degradation rates were dependent on the MEA tested and not significantly affected by the cell temperatures used in this work. Because of the wide range of observed degradation rates it became apparent that degradation rates needed to be determined in-situ, i.e. during the contamination experiment, for each MEA and operating condition.

Several similar 200 h experiments were analyzed to determine the fraction of time of the experiment required to accurately extrapolate cell performance over the entire duration of the experiment. The data were fit over different fractions of time using Eq. (3). All fits started at the beginning of the experiment and ranged from 1/6 to the entire experiment time, e.g. from 33 to 200 h for a 200 h experiment. Fits were subsequently extrapolated over the entire duration of the test.

Fig. 11 shows a representative example experiment performed at 80 °C and an anode inlet humidity of 80%. The figure shows a comparison of the cell voltage data with data extrapolated from the different fitting ranges. The voltage data fit to the entire duration of the experiment showed excellent agreement with the measured voltage and emphasized the accuracy of the fitting equation. As the amount of data used for fitting, i.e. the fitting

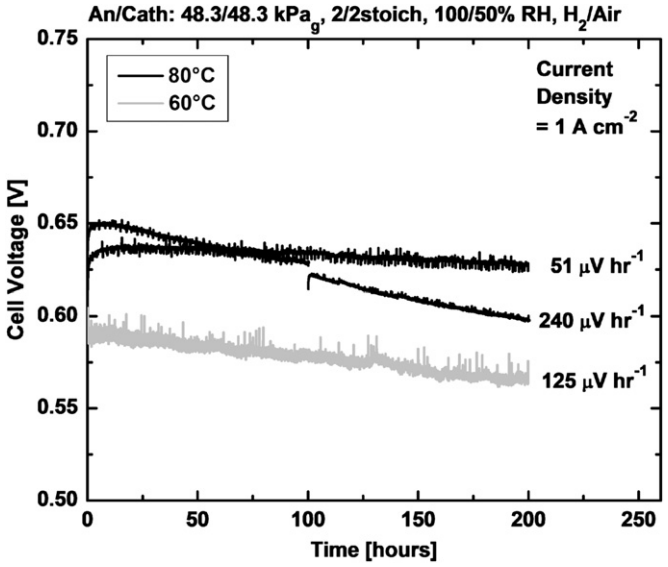

Fig. 10. Cell voltage versus time for different operating conditions with neat H_2/air

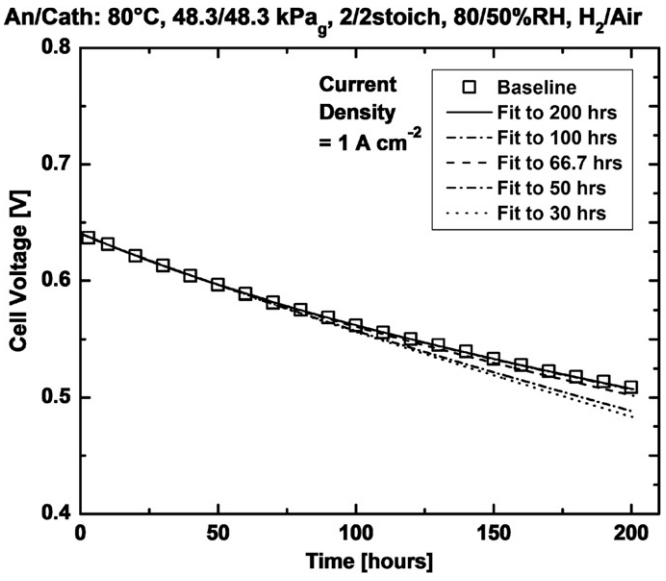

Fig. 11. Extrapolations of data fit with Eq. (3) from different time intervals of the experiment for cell operated for 200 h at 80 °C and an anode/cathode inlet relative humidity of 80/50%. All fits start from $t = 0$.

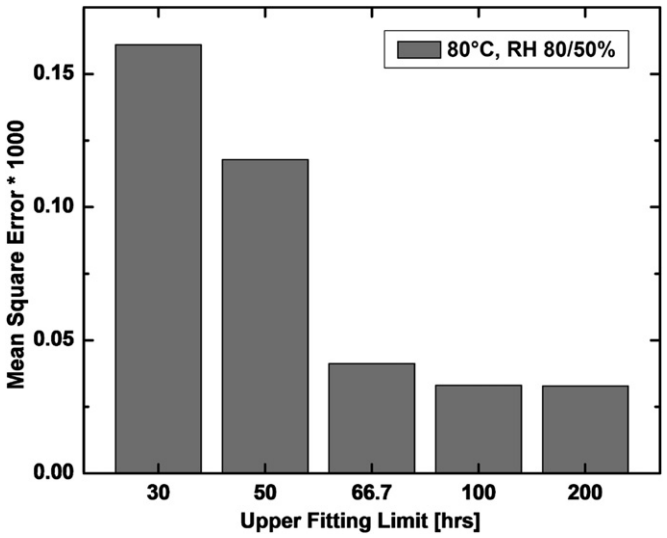

Fig. 12. Mean square error associated with extrapolation from fits of the five time intervals in Fig. 13 for cell operated for 200 h at 80 °C and an anode/cathode inlet relative humidity of 80/50%.

Table 4
Operating conditions, contaminant exposure time ranges, fitting time ranges, employed fitting equations, and fitting parameter and R^2 values of conducted experiments and fits.

An/Ca conditions	Current density [A cm^{-2}]	CO concentration [ppm]	Poisoning time range [h]	Fitting equation	Fitting range [h]		p_1	p_2	p_3	p_4	p_5	R^2
					Contamination	Recovery						
60 °C 48.3/	1	1	45.27–100.27	17	8.6–100.27		−0.00025	0.17308	59.22434	17.37171		0.99918
48.3 kPa$_g$2/2				22		0–45	0.00601	0.05984	−0.27753	−0.81608	0[a]	0.99852
stoich	1	2	40.27–90.27	17	4–90.27		−0.0002	0.2453	46.91563	36.08006		0.99892
100/50%RH				22		0–40	0.00333	0.04822	−0.11465	−0.74199	0[a]	0.9977
	1	10	40.4–70.49	18	39.27–41.2		0.00005	4.82588	39.77731	0.56744		0.99846
				19	41.14–50		0.27662	−0.00435	41.12917	0.04305		0.99653
				20	49–70.49		0.28428	9.77387E−4				0.91612
				22		0–40	−0.0071	0.08584	−0.04685	−0.47243	0[a]	0.99318
80 °C 48.3/	1	1	50.27–130.27	17	22.5–130.27		−0.00017	0.02566	62.39081	14.27875		0.98897
48.3 kPa$_g$2/2				22		0–40	0.0097	0.0199	−1.03109	−0.96593	0[a]	0.92548
stoich	1	2	40.27–90.27	17	6.5–90.27		−0.00011	0.04463	45.76363	27.5232		0.99855
100/50%RH				22		0–26.1	−0.00216	0.0194	−0.13905	−0.47695	0[a]	0.96912
	1	10	40.27–70.27	18	4–42.17		0.00006	5.80598	39.68907	−1.05889		0.99652
				19	42.15–70.27		0.20752	−0.00007	42.11886	0.01257		0.9635
				22		0–40	0.00664	0.01848	−0.04652	−0.82592	0[a]	0.98442
80 °C 48.3/	1	1	45.27–100.27	17	1–100.27		−0.00012	0.02473	53.85678	18.83773		0.99782
48.3 kPa$_g$2/2				22		0–45	−0.00078	0.01825	−0.65148	−0.63686	0[a]	0.95346
stoich	1	2	40.27–90.27	17	2–90.27		−0.00013	0.04853	46.63424	24.76019		0.99757
80/50%RH				22		0–40	0.00945	0.0186	−0.52559	−1.19436	0[a]	0.9555
	1	10	40.38–70.48	18	4–41.92		0.00003	7.34888	39.98319	−1.60282		0.99619
				19	41.92–52		0.18768	−0.00059	41.89154	0.02101		0.96391
				20	52–70.48		0.19123	7.52365E−4				0.88771
				22		0–40	0.01023	0.02192	−0.02485	−0.65766	0.00035	0.99403
80 °C 48.3/	1	1	50.27–130.27	18	27.3–56		0.00032	1.01504	51.73667	−0.09594		0.89508
48.3 kPa$_g$2/2				17	53–130.27		−0.01211	0.02772	59.30433	6.59218		0.98808
stoich				22		0–30	0.00812	0.1905	−3.70526	−1.75432	0[a]	0.98852
60/50%RH	1	2	40.27–70.27	17	16–70.27		−0.00028	0.07737	46.33266	25.75828		0.99896
				22		0–40	0.00524	0.02661	−0.19723	−0.65537	0[a]	0.99405
	1	10	28.94–58.94	18	28.94–30.5		0.00003	7.11219	28.39885	−1.44645		0.99725
				19	30.5–58.94		0.26882	−0.00049	30.49458	0.02182		0.98302
				22		0–40	−0.00085	0.01974	−0.03141	−0.80609	0[a]	0.99698
60 °C 48.3/	0.2	2	85.18–215.18	17	5–215.18		0.00006	0.01876	117.99301	11.69972		0.99593
48.3 kPa$_g$2/2	0.6	2	50.38–120.6	20	5–51.65		0	0				
stoich				21	51.65–68.6		0.02164	0.00493	58.48721	0.00016	2.1309E−6	0.99965
100/50%RH				17	68.6–120.6		−2	0.15948	53.90687	155,733		0.93051
				22		0–30	0.00393	0.05023	−0.24847	−0.83531		0.99907

[a] Forced value.

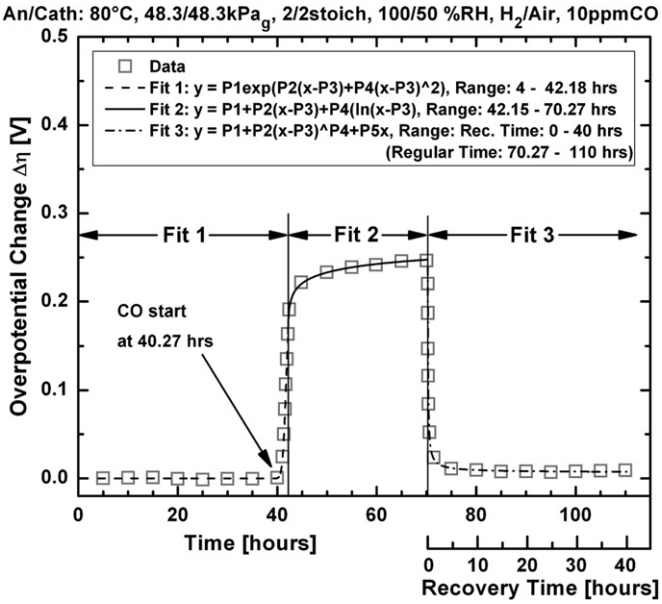

Fig. 13. Fitting example for contaminant experiment with dry gas concentration of 10 ppm CO at 80 °C with an anode/cathode inlet relative humidity of 100/50%. The example data was partitioned into three fitting sections covering: (i) the pre-poisoning phase and the beginning of transient response of the poisoning phase, (ii) the remainder of the poisoning phase including the steady state poisoning state, and (iii) the recovery phase.

range, was decreased, however, the accuracy of the extrapolation decreased.

To determine the fraction of experiment time necessary to provide a reasonably accurate extrapolation the mean square error (MSE) of the measured voltage data to the data extrapolated from the fit was calculated for each fitting range using Eq. (11). Fig. 12 shows the MSEs for the data and fits shown in Fig. 11. The data indicated that the MSE of the extrapolated data significantly improved when the fitting range was at least one third of the entire test duration.

$$\mathrm{MSE} = \frac{\sum_{i=1}^{n}[V_{\mathrm{Cell}}(t_i) - V_{\mathrm{Fit}}(t_i)]^2}{n} \tag{11}$$

Appendix B. Mathematical data description for modeling efforts

Research institutions throughout the world are working on the impact of contaminants on fuel cell performance and many contribute to national and international efforts to develop a purity standard for hydrogen used in PEMFC applications, specifically PEMFC vehicle applications. Low-level contaminant experiments and contaminant model development are essential for the success of this effort. In this section we report our data to the research community to make it available for model development efforts. The overpotential change of the cell, $\Delta\eta$, for each experiment is reported using the mathematical expressions Eqs. (12)–(17). While these equations and their fitting parameters do not contain any physical meaning, they served as a convenient medium to transfer the large amount of experimental data presented and discussed in this work.

$$y = p_2 + (p_1 - p_2)/(1 + (x/p_3)^{p_4}) \tag{12}$$

$$y = p_1 \cdot \exp\left(p_2 \cdot (x - p_3) + p_4 \cdot (x - p_3)^2\right) \tag{13}$$

$$y = p_1 + p_2 \cdot (x - p_3) + p_4 \cdot \ln(x - p_3) \tag{14}$$

$$y = p_1 + p_2 \cdot x \tag{15}$$

$$y = p_1 + p_2 \cdot (x - p_3) + p_4 \cdot (x - p_3)^2 + p_5 \cdot (x - p_3)^4 \tag{16}$$

$$y = p_1 + \left(p_2 \cdot (x - p_3)^{p_4}\right) + p_5 \cdot x \tag{17}$$

Table 4 lists the operating conditions, contaminant exposure time ranges, fitting time ranges, employed fitting equations, and fitting parameter values of all conducted experiments, and the R^2 value of the fits. With this information the $\Delta\eta$ versus time of each experiment can be accurately reconstructed. Note that (i) data values prior to contaminant exposure can be set to zero, and (ii) extrapolation of the fits beyond the indicated fitting ranges will likely result in significant deviation from the measured values. Fig. 13 shows an example for fitting the $\Delta\eta$ of an experiment using three equations: (i) the exponential Eq. (13) was employed to describe the pre-poisoning phase and the beginning of the non-steady state ranging from 4 to 42.17 h, (ii) Eq. (14) which contained linear and logarithmic terms was employed to describe the remainder of the non-steady state and the steady poisoning state period ranging from 42.17 to 70.27 h, and (iii) Eq. (17) which contained linear and power terms was used for cell performance recovery ranging from 70.27 to 100.27 h. The recovery time is shown as a second time scale in Fig. 13 which starts at a time of zero. This time scale should be used when reproducing the data and was employed to maximize the fitting accuracy of the cell performance recovery.

Glossary

Symbols

MSE	mean square error
n	number of data points
p_1, p_2, p_3, p_4	fitting parameter
Q_{CBal}	quality of carbon balance
t_{arb}	arbitrary chosen saturation time
t	time
t_{sat}	time required to reach saturation of catalyst layer with contaminant
t_{ss}	time steady state poisoning state is reached
t_{stop}	time contaminant exposure stops
V_{cell}	cell voltage
V_{fit}	fitted voltage
$\Delta\eta$	overpotential change
ξ_{CO}	magnitude of CO conversion

References

[1] W.H.J. Hogarth, J.C.D. da Costa, G.Q.M. Lu, J. Power Sources 142 (2005) 223.
[2] T.R. Ralph, Platinum Met. Rev. 43 (1999) 14.
[3] X. Cheng, Z. Shi, N. Glass, L. Zhang, J. Zhang, D. Song, Z. Liu, H. Wang, J. Shen, J. Power Sources 165 (2007) 739.
[4] T.E. Springer, T. Rockward, T.A. Zawodzinski, S. Gottesfeld, J. Electrochem. Soc. 148 (1) (2001) A11.
[5] J. St-Pierre, J. Electrochem. Soc. 156 (3) (2009) B291–B300.
[6] SAE TIR J2719, Hydrogen Specification Guideline For Fuel Cell Vehicles (November 2005).
[7] G. Bender, M. Angelo, K. Bethune, S. Dorn, T. Thampan, R. Rocheleau, J. Power Sources 193 (2009) 713.
[8] Y. Zhai, G. Bender, S. Dorn, M. Angelo, K. Bethune, R. Rocheleau, ECS Trans. 16 (2) (2008) 873–880.
[9] F.A. Uribe, S. Gottesfeld, T.A. Zawodzinski, J. Electrochem. Soc. 149 (3) (2002) A293–A296.
[10] R. Halseid, PJ.S. Vie, R. Tunold, J. Power Sources 154 (2006) 343–350.
[11] J.J. Baschuk, X. Li, Int. J. Energy Res. 25 (2001) 695–713.
[12] G.A. Camara, E.A. Ticianelli, S. Mukerjee, S.J. Lee, J. McBreen, J. Electrochem. Soc. 149 (6) (2002) A748.
[13] S. Jiménez, J. Soler, R.X. Valenzuela, L. Daza, J. Power Sources 151 (2005) 69–73.

[14] T. Gu, W.-K. Lee, J.W. Van Zee, Appl. Catal. B: Environ. 56 (2005) 43–49.
[15] T. Kawaguchi, W. Sugimoto, Y. Murakami, Y. Takasu, Abs. 31, 206th Meeting of the Electrochemical Society, 2004.
[16] T. Ioroi, K. Yasuda, Y. Miyazaki, Phys. Chem. Chem. Phys. 4 (2002) 2337–2340.
[17] J. Zhang, T. Thampan, R. Datta, J. Electrochem. Soc. 149 (6) (2002) A765.
[18] T.R. Ralph, M.P. Hogarth, Platinum Metals Rev. 46 (3) (2002) 117–135.
[19] V.I. Basura, C. Chuy, P.D. Beattie, S. Holdcroft, J. Electrochem. Soc. 501 (2001) 77–88.
[20] S. Ma, E. Skou, Solid State Ionics 178 (2007) 615–619.
[21] K. Broka, P. Ekdunge, J. Appl. Electrochem. 27 (2) (1997) 117.
[22] J.Y. Shim, S. Tsushima, S. Hirai, J. Electrochem. Soc. 156 (6) (2009) B690–B694.